Raman spectroscopy and x-ray diffraction of phase transitions in Cr_2O_3 to 61 GPa

Sang-Heon Shim*
Department of Earth, Atmospheric, and Planetary Sciences, Massachusetts Institute of Technology, Cambridge, Massachusetts 02139, USA

Thomas S. Duffy
Department of Geosciences, Princeton University, Princeton, New Jersey 08544, USA

Raymond Jeanloz
Department of Earth and Planetary Sciences, University of California, Berkeley, California 94720, USA

Choong-Shik Yoo and Valentin Iota
Lawrence Livermore National Laboratory, Livermore, California 94551, USA

(Received 2 October 2003; revised manuscript received 24 December 2003; published 6 April 2004)

Raman spectroscopy and x-ray diffraction measurements have been performed for pure Cr_2O_3 to 61 GPa at ambient temperature with and without laser heating. Several changes were found at 15–30 GPa under cold compression: splittings of two E_g phonons, steep selective increase of some phonon intensities, softening of low-frequency phonon modes, selective broadening of some diffraction lines, systematic deviation of diffraction positions relative to the corundum structure assignment, and eventual splitting of the $(110)_H$ diffraction line at 58 GPa. These changes are consistent with those expected for a phase transition to the monoclinic V_2O_3-type ($I2/a$) structure. Another phase transition has been found above 30 GPa after laser heating. This is accompanied by considerable changes in Raman spectra and diffraction patterns, which implies that the transition is reconstructive. The diffraction patterns of this phase can be well explained by either of the orthorhombic structures, perovskite or Rh_2O_3-II type. This confirms the recent prediction of stability of an orthorhombic phase in Cr_2O_3 at high pressure by first-principles calculations. Color changes of Cr_2O_3 were also detected: from green to red at 14 GPa during cold compression and from red to green during the phase transition to the orthorhombic phase above 30 GPa. Detailed analyses on diffraction patterns show that the color changes are relevant to Cr-O bond-length change. Furthermore, the observed variation trends of bond lengths in Cr_2O_3 during cold compression are similar to those in Al_2O_3 with much more pressure sensitivity, which is consistent with recent first-principles calculations, but are opposite to those in V_2O_3 and Fe_2O_3 at high pressure.

DOI: 10.1103/PhysRevB.69.144107 PACS number(s): 61.50.Ks, 61.10.Nz, 78.30.−j, 75.50.Ee

I. INTRODUCTION

$3d$-transition metal sesquioxides have attracted a great deal of attention with regard to their electromagnetic properties and structural changes.[1] Whereas many of these sesquioxides (M_2O_3, M = Ti, V, Cr, Fe) have the corundum structure ($R\bar{3}c$, D_{3d}^6) at ambient conditions, various types of transitions have been reported for different sesquioxides at high pressure and high temperature with different changes in crystal structure, or electromagnetic properties: No crystallographic changes occur for the insulator-to-semiconductor transition in Ti_2O_3 at 390–470 K and ambient pressure.[2,3] In $(V_{1-x}Cr_x)_2O_3$ ($x=0.0$–0.12), a structural transition to a monoclinic phase ($I2/a$, C_{2h}^6) is accompanied with a transition from a paramagnetic semiconductor to an antiferromagnetic insulator at low temperature or high pressure depending on composition.[4,5] Fe_2O_3 transforms to a metallic orthorhombic phase (Rh_2O_3-II or perovskite type) at 55 GPa (Refs. 6 and 7). Thus, investigation of Cr_2O_3 at high pressure is of interest to further explore structural changes in the transition metal oxides.

A phase transition in Al_2O_3 from the corundum to the Rh_2O_3-II structures at 78 GPa was proposed on the basis of first-principles calculations.[8] A later x-ray diffraction study[9] reported changes at 100 GPa which could be interpreted as evidence for this transition. However, the resolution of the diffraction patterns was not sufficient to be conclusive. In the proposed mechanism for the phase transition in ruby (Cr-doped Al_2O_3), CrO_6 octahedra in the ruby structure are thought to be the critical units that trigger the phase transition.[10] Since ruby is widely used as a pressure calibrant in high-pressure studies, understanding the nature of ruby phase transitions is of broad interest. Another first-principles calculation[11] also predicts that pure Cr_2O_3 may transform to the Rh_2O_3-II structure at much lower pressure, 15 GPa. While Raman spectra[12] have shown clear evidence for an unknown structural transition above 13 GPa, x-ray-diffraction studies[12,13] have not found any evidence for the structural change to 30 GPa. This discrepancy has not been resolved.

Here we present the results of measurements using Raman spectroscopy and x-ray diffraction and visual observations for pure Cr_2O_3 to 61 GPa at 300 K with and without laser

 ©2004 The American Physical Society

heating. Several lines of evidence for a phase transition at 15–30 GPa were found when Cr_2O_3 is compressed at 300 K. We also report the Raman spectra and diffraction patterns of the orthorhombic phase observed after laser heating above 30 GPa. We will discuss the crystal structures of the high-pressure phases and structural response of Cr_2O_3 to stress.

II. EXPERIMENTAL TECHNIQUES

Pure synthetic Cr_2O_3 (Aldrich, 99.995%) was used as starting material. The purity and crystal structure (corundum type) were confirmed using x-ray diffraction and Raman spectroscopy at ambient conditions. Powdered Cr_2O_3 was loaded in the 100 μm hole of an indented stainless steel gasket and compressed between two 300 μm culet low-fluorescence diamond anvils. A symmetric-type diamond cell with 60° conical apertures and a Mao-Bell-type diamond cell with slot shaped apertures were used. Small ruby chips were loaded for pressure measurements using the quasihydrostatic ruby pressure scale.[14] Argon was cryogenically loaded into the sample chamber as a pressure transmitting and thermal-insulating medium. For Raman measurements below 10 GPa, we used a methanol-ethanol (4:1) mixture as a pressure medium.

Raman spectra were excited using an argon-ion laser ($\lambda = 514.5$ nm) and recorded with a single spectrometer at Princeton University[7] and with a triple spectrometer at Livermore National Laboratory. A spectral range of 150–1250 cm^{-1} was used for measurements to 62 GPa. The spectrometers were frequently calibrated using Ne emission spectra over the course of the experiments. In order to prevent sample heating by the argon-ion laser, we loaded the sample directly in contact with a high thermal-conductivity diamond anvil and measured spectra from this contact surface. For laser heating experiments, we separated the sample foils from the diamond anvils by loading argon below and above the samples to reduce heat loss through the anvils. Raman spectra were typically collected over 10 min. Peaks were fitted using a Lorenzian profile shape function. For asymmetric peaks we used a split Pearson VII function.

Angle-dispersive x-ray diffraction measurements were performed at the B2 sector of the Cornell High Energy Synchrotron Source (CHESS) and at the 10.3 sector of the Stanford Synchrotron Radiation Laboratory (SSRL) using monochromatic x-ray beams ($\lambda = 0.4959$ Å at CHESS and 0.7277 Å at SSRL) and imaging plates. Two diffraction patterns were measured at each pressure at different distances from the sample. The sample-imaging plate distances were measured using the diffraction lines of NaCl and MgO. The backing plates of the symmetric cell restricted the maximum value of 2θ to $\sim 16°$. In order to obtain a wider angle range, we tilted the symmetric type diamond cell with respect to the incident x-ray beam. This allows us to measure spectra to $\sim 28° 2\theta$. However, instead of full diffraction rings, we obtained partial rings (160° arc) due to the tilting. With the Mao-Bell-type cell, since it has a slot aperture, we were able to measure diffraction patterns to $\sim 40° 2\theta$ without tilting. However, the slot-type aperture only allows 8°–10° arc of diffraction rings. In these experiments, pressure was measured using the argon equation of state[15] in addition to the ruby scale. Some of samples were heated using a cw Nd:YAG laser (where YAG stands for yttrium aluminum garnet). The entire sample was scanned by the laser for 15–20 min to anneal differential stresses or synthesize a high-temperature phase.

Geometric corrections for the measured diffraction images were performed using the program SIMPA.[16] Integrations to obtain one-dimensional patterns were carried out for the portion of the rings ($\sim 60°$) where the maximum 2θ angle range is achieved for the patterns measured with the symmetric-type cell. Individual peak fitting using a pseudo-Voigt profile function was performed to obtain the unit-cell parameters. Unit-cell refinements were performed using the UNITCELL code.[17] GSAS (Ref. 18) was used for Rietveld refinement and Le Bail fitting.

We also performed energy-dispersive x-ray diffraction measurements at *in situ* high *P-T* (25–30 GPa and 1500–2000 K) at the GSECARS sector of the Advanced Photon Source. A double-sided laser heating system[19] with a cw Nd:YLF laser was used in this experiment.

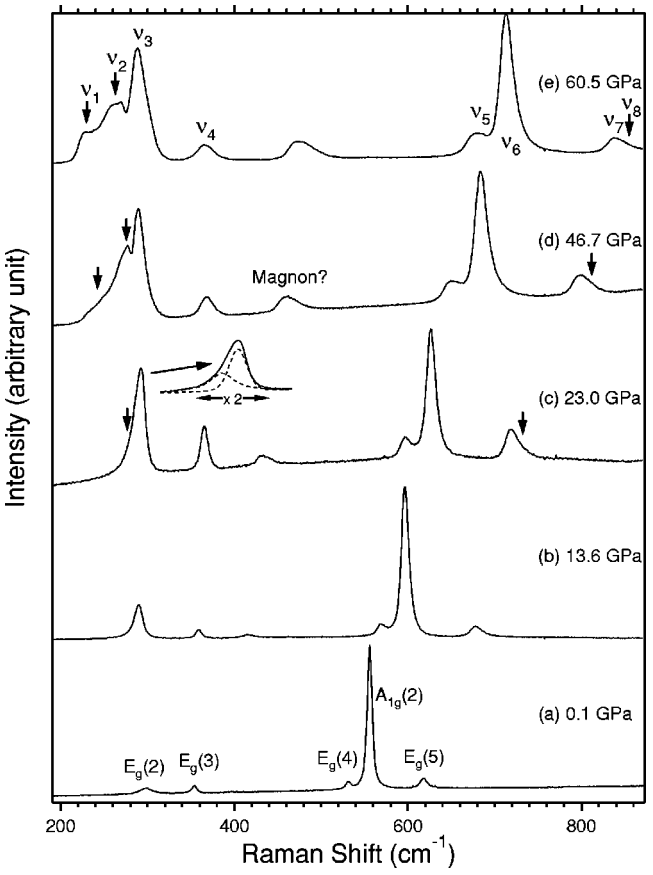

FIG. 1. High-pressure Raman spectra of Cr_2O_3 measured at 300 K without laser heating. Peak assignments for the corundum-type phase follow from single-crystal measurements (Ref. 21). New features observed above 15–30 GPa during cold compression are indicated by arrows (ν_1, ν_2, and ν_8). An example for the peak fit for $E_g(2)$ using two peaks (ν_2 and ν_3) is shown (dashed lines) together with the observed spectrum (solid line) in the inset. Pressure is shown above each trace.

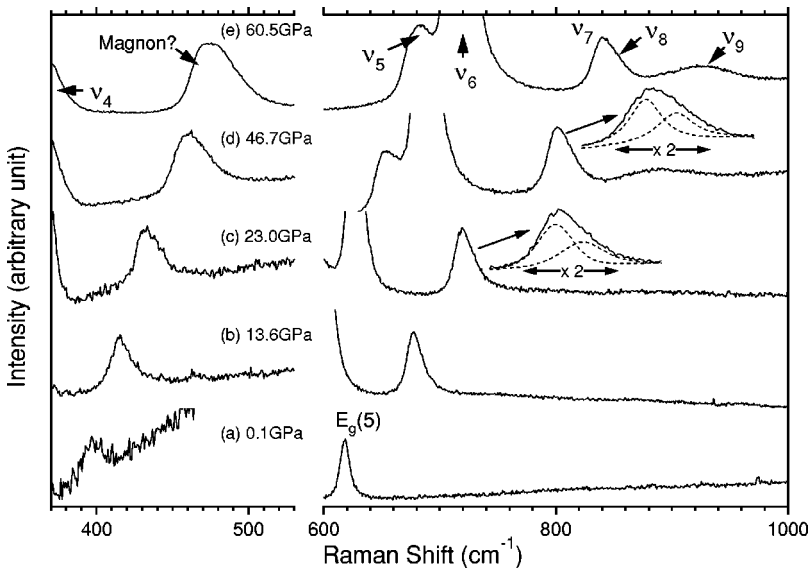

FIG. 2. Raman spectra of the mode at 400–450 cm^{-1}, which has been assigned as a magnon in previous studies (Ref. 21), and selected phonon modes at 600–1000 cm^{-1} at high pressures and ambient temperature. Examples for the peak fit for $E_g(5)$ using two peaks (ν_7 and ν_8) are shown (dashed lines) together with the observed spectra (solid lines) in the insets. Notation is the same as in Fig. 1.

III. RESULTS

A. Phase transition at 15–30 GPa and 300 K

Raman spectra were measured to 60.5 GPa at 300 K without heating (Figs. 1–3). We compare the measured Raman shifts at the lowest pressure (0.09 GPa) with previous ambient pressure studies in Table I. The different studies are generally in agreement within a few wave numbers. Two different single-crystal polarization measurements[20,21] agree on the mode assignment except for a mode in the 290–304 cm^{-1} range. We use the assignment[21] which is consistent with that for $V_{1-x}Cr_xO_3$ (Ref. 22). Two weak modes below 270 cm^{-1} were not observed in our powder Raman spectra as was also the case for other powder Raman studies.[12,23]

With compression, we observed a relative intensity increase [Figs. 1(a), 1(b), and 4] and frequency decrease (Fig. 3) of $E_g(2)$ mode to 15 GPa. Above 15 GPa, two phonon modes $E_g(2)$ and $E_g(5)$ become asymmetric [see the insets of Figs. 1(c) and 2(c), and Fig. 3]. Upon further compression, clear splitting of $E_g(2)$ into a doublet (ν_2 and ν_3) was observed, and a broad band (ν_1) also appears at $\sim$250 cm^{-1} above 26 GPa [Figs. 1(d), 1(e), and 3]. Mougin *et al.*[12] observed this splitting as well, but incorrectly attributed it to pressure gradients in the sample. While we were not able to

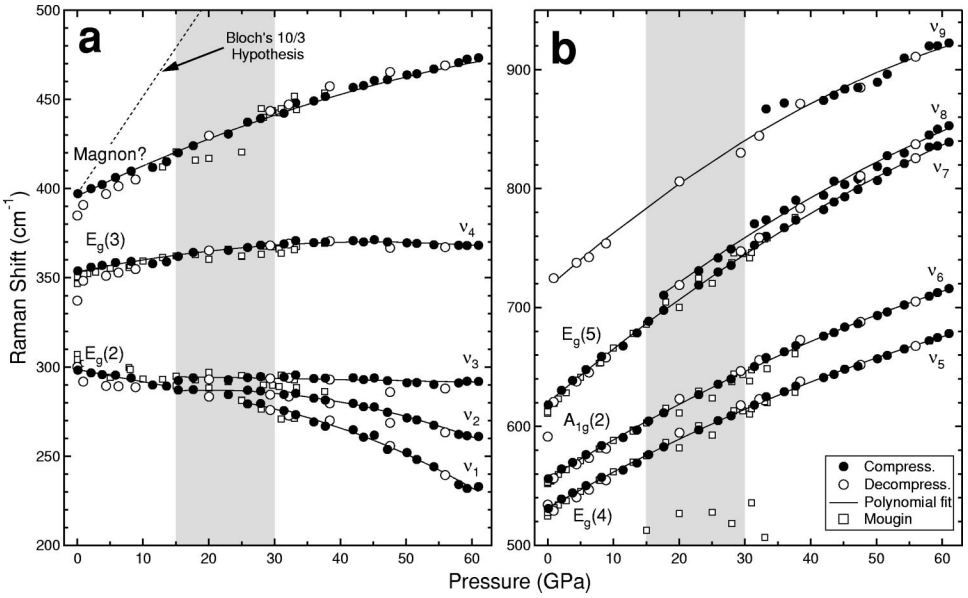

FIG. 3. Pressure shift of Raman modes at high pressure and 300 K without laser heating. Solid circles are the data points for compression and open circles are for decompression. Polynomial fits for compression data are shown as solid lines. The polynomial fit for ν_9 also includes decompression data points. Lower pressure Raman measurements (Ref. 12) are plotted for comparison (open squares). Assignments follow from single-crystal polarization measurements (Ref. 21). The predicted magnon frequency change with compression by Bloch's hypothesis (Ref. 25) is plotted as a dashed line in (a). The shaded area indicates where changes in Raman spectra were detected during cold compression and decompression. Peak assignments are the same as in Fig. 1.

TABLE I. Raman modes of Cr_2O_3 at ambient condition.

Ref. 20		Ref. 21		Ref. 23	Ref. 12	This study[a]	$(V_{1-x}Cr_x)O_3$ (Ref. 22)[b]	
		E_g	235				E_g	210
		A_{1g}	266				A_{1g}	234
A_{1g}	303	E_g	290	304	296	298	E_g	246
E_g	351	E_g	352	353	350	354	E_g	327
E_g	397	Magnon	396	401		397	Magnon	440[c]
E_g	530	E_g	528	529	529	531		
A_{1g}	551	A_{1g}	547	553	554	556	A_{1g}	501
E_g	609	E_g	617	616	615	618	E_g	595

[a]Measured at 0.09 GPa.
[b]For $x \leqslant 0.03$ at ambient condition.
[c]At 80 K for antiferromagnetic insulator phase.

observe splitting for $E_g(5)$, the increase of asymmetry and the broadness of this mode compared to other observed modes imply that this band may be at least a doublet above 17 GPa (Fig. 2). In fact, fitting with a doublet improves the goodness of fit significantly [see the inset of Fig. 2(c) and 2(d)]. Together with these changes, it is also observed that the spectral background increases above 15 GPa. Significant intensity changes were also detected at 15–30 GPa for $E_g(2)$, $E_g(3)$, and $E_g(5)$ modes (Fig. 4) in agreement with Ref. 12. All these changes are confirmed to be reversible upon decompression (Fig. 3) except that ν_9 survived down to ambient pressure. All phonon modes show significant nonlinear behaviors at high pressure, which was also seen in Raman spectra of Fe_2O_3 (Ref. 7). In addition, the four low-frequency modes (ν_1–ν_4) show significant softening at high pressure.

Since powder Raman spectroscopy is not sufficient to determine a crystal structure directly, we investigated analog systems. We consider the monoclinic phase (C_{2h}^6) observed at low temperature and ambient pressure in pure and Cr-doped V_2O_3 (Refs. 22 and 24), and the orthorhombic phases (Rh_2O_3-II or perovskite type, Ref. 7) which have been reported for other sesquioxides. Relatively minor changes in vibrational spectra can be expected for the monoclinic structure as it is essentially a slightly distorted corundum structure. However, it has been observed for Fe_2O_3 that a phase transition to the orthorhombic phase is reconstructive and is accompanied by extensive changes in Raman spectra.[7] In fact, the observed changes in Raman spectra at 15–30 GPa and ambient temperature are significantly different from the spectra of the orthorhombic phase of Cr_2O_3 measured above 30 GPa and after laser heating (see Sec. III B). Furthermore, the changes in the Raman spectra of Cr_2O_3 at 15–30 GPa are more consistent with those of the trigonal-monoclinic phase transition in pure and Cr-doped ($Cr<0.03$) V_2O_3 where peak splittings were observed for all E_g modes.[22,24] The splittings of E_g modes are also consistent with the group theoretical prediction for the transition.

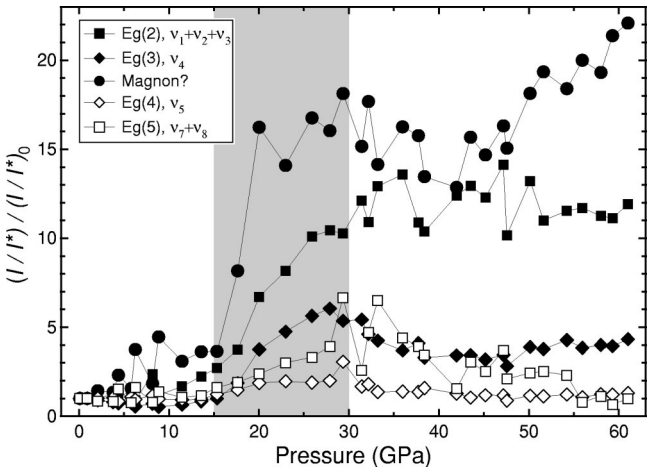

FIG. 4. Normalized relative intensities of Raman modes at high pressure. Intensities are obtained by integrating areas under peaks after subtracting background. Relative intensities are obtained by dividing the intensities by the $A_{1g}(2)$ or ν_6 intensity (I^*). Normalization is performed using the measurement at the lowest pressure (0.09 GPa), $(I/I^*)_0$.

In this study, we observed splittings for only two E_g modes (Figs. 1–3). In high-pressure experiments, stress inhomogeneity increases upon compression resulting in a peak broadening, and this could prevent detection of small peak splittings at high pressures. In fact, $E_g(4)$ is partly overlapped by a much stronger A_{1g} mode. In Cr_2O_3, $E_g(2)$ becomes a triplet instead of doublet as observed in pure or Cr-doped V_2O_3. Since an E_g mode is doubly degenerate, one of this observed triplet can be attributed to the appearance of a new mode. In fact, group theory predicts not only new Raman-active modes from the splitting of the Raman-active phonons of the corundum phase but also the appearance of new Raman-active phonons from the inactive modes of the corundum phase.

A Raman mode was also observed at 397 cm^{-1} at ambient pressure and this was also readily measured at high pressures (Figs 2 and 3). This mode has been assigned to one-magnon scattering based on a steep intensity decrease observed near the Néel temperature (308 K) and its good agreement with inelastic neutron scattering.[21] This mode is continuously observed throughout the experimental range and, moreover, the relative intensity shows a steep increase at 15–30 GPa (Fig. 4). This increase is the greatest among

the observed intensity jumps in this pressure range. In addition, this peak becomes asymmetric above 20 GPa (Fig. 2).

Bloch[25] has proposed that the mode Grüneisen parameter γ for magnons may be close to 10/3. We calculated the expected variation of the Raman frequency ν if this hypothesis is valid for Cr_2O_3, using the following equation:

$$\gamma = -\frac{d\ln\nu}{d\ln V} = \frac{K_T}{\nu}\left(\frac{d\nu}{dP}\right). \quad (1)$$

The bulk modulus K_T ranges from 230 to 240 GPa (Refs. 26 and 27). The lower bound result for the pressure behavior of this mode is shown in Fig. 3(a), provided that the mode is due to magnon-photon interaction and follows Bloch's hypothesis. The observed pressure variation of the mode is very different from what is expected from Bloch's hypothesis, and its Grüneisen parameter is calculated to be 1.06 ± 0.03 from our data.

Bloch's hypothesis is based on a variety of empirical trends. However, the accessible pressure range was limited at that time. Recently it has been shown that the magnon γ ranges from 1.6 to 3.3 and may be material dependent in contrast to Bloch's hypothesis: 1.7–2 for La_2CuO_4 (Ref. 28), 2.7 ± 0.2 for CoO (Ref. 29), and 2.3–2.6 for NiO (Ref. 30). In fact, Bloch's hypothesis considers only up to second neighbor interactions, whereas it has been shown that the relatively complicated corundum-type lattice requires to take into account up to fourth neighbor interactions.[31] It is notable that $\gamma = 1.06$ is the lowest ever reported for magnons and a significant nonlinearity of the pressure-induced shift is observed.

However, we cannot rule out a phonon assignment for this mode. Its mode γ is very close to other phonon mode γ's. One possibility is that a new phonon mode appears due to the phase transition and its frequency coincides with the magnon. However, it should be noted that γ is already very low even below the phase transition pressure [Fig. 3(a)].

We also observed a broad band near 700 cm^{-1} above 30 GPa during compression which is preserved upon decompression [ν_9 in Figs. 2 and 3(b)]. A similar feature was observed near this range in $(Fe_{1-x}Cr_x)_2O_3$ ($x = 0.0$–0.8, Refs 23 and 7) and assigned as an IR-active and Raman-inactive mode that appeared in Raman spectra due to surface- or pressure-induced defects. An IR measurement at ambient pressure[32] reported features near this range [$E_u(TO) = 734$ cm^{-1} and $A_{2u}(\mathrm{TO}) = 726$ cm^{-1}]. The extrapolated value at ambient pressure for this mode is 717 cm^{-1}, which shows a reasonable agreement with the IR-active mode considering its broad and weak nature.

X-ray diffraction patterns have been measured at CHESS to 58 GPa at 300 K without laser heating. Below 15 GPa, no significant change in diffraction patterns was found and all diffraction lines were well fitted with those of the corundum structure ($R\bar{3}c$) [Fig. 5(a)]. However, above 30 GPa, some peaks are selectively broadened: the full width at half maximum (FWHM) of $(110)_H$ and $(116)_H$ is a factor of 3 and FWHM of $(104)_H$ and $(024)_H$ is a factor of 2 greater than that of $(012)_H$ diffraction line. In addition, systematic errors were found above 30 GPa in unit-cell parameter refinements

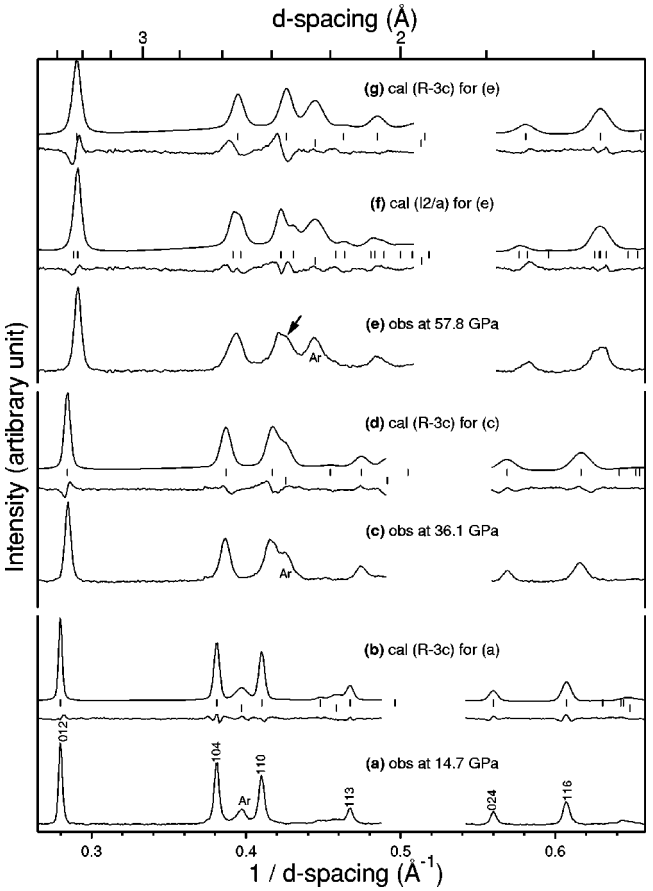

FIG. 5. Observed (a,c,e) and calculated (b,d,f,g) x-ray-diffraction patterns at high pressure. The difference between the observed and calculated patterns is also shown for each calculated pattern. Tick marks are the diffraction peak positions for Cr_2O_3 [corundum phase at the top of (b), (d), and (g); monoclinic V_2O_3 phase at the top of (f)] and Ar [bottom of (b), (d), (f), (g)]. Backgrounds were subtracted. Hexagonal Miller indices are given for the major lines of Cr_2O_3 for the pattern measured at 14.7 GPa (a). For the observed pattern at 57.8 GPa (e), we show two different refinements with the corundum-type ($R\bar{3}c$) (g) and the monoclinic V_2O_3-type ($I2/a$) (f) structures. The arrow indicates the peak splitting.

when the corundum-type structure is assumed. The maximum errors occurred for $(110)_H$ and $(116)_H$ which are the broadest lines above 15 GPa and this increases with compression. At the maximum pressure (58 GPa), we were able to observe a peak splitting of the $(110)_H$ line [Fig. 5(e)].

We performed Rietveld refinements with two different crystal structure models (corundum type, $R\bar{3}c$, and monoclinic V_2O_3 type, $I2/a$) for the entire x-ray data set measured without laser heating. Below 15 GPa, the corundum type fits well the observed diffraction patterns. However, systematic differences were found between the calculated and observed intensities above 30 GPa after the refinements with the corundum structure: the corundum type predicts lower d spacings for $(012)_H$ and higher d spacings for $(104)_H$ and $(110)_H$ than the observed patterns [Figs. 5(b), 5(d), and 5(g)]. This is the same trend observed in the unit-cell refinements for individual peak fitting results. However, use of the monoclinic

V_2O_3 structure decreases the systematic differences between the observed and calculated diffraction patterns, and the difference is much more random [Fig. 5(f)].

We also examined the Rh_2O_3-II-type structure ($Pbna$), which is proposed by first principles calculations for a high-pressure phase of Cr_2O_3 (Refs. 10 and 11), and the perovskite structure ($Pbnm$), which is proposed as a high-pressure phase of Fe_2O_3 (Ref. 33), by calculating diffraction patterns at corresponding pressures. However, neither of these structures are consistent with the observed subtle changes. Indeed, the observed diffraction patterns after laser heating above 30 GPa, which can be well explained by an orthorhombic unit cell, demonstrate that the diffraction pattern of the orthorhombic phase is considerably different from the observed diffraction patterns above 15–30 GPa without laser heating (see Sec. III B).

The unit-cell parameters obtained from Rietveld refinements were plotted in Fig. 6. To facilitate direct comparison, we transformed the trigonal and monoclinic cell parameters to hexagonal and pseudohexagonal cell parameters, respectively (the transformation matrix can be found in Ref. 5). Below 15 GPa, our refinement results with the trigonal lattice (corundum structure) agree well with previous studies.[13,26,34] However, above 30 GPa, our results for both trigonal cell and monoclinic cell refinements start to deviate from the extrapolation of hydrostatic compression data measured at lower pressure[26,27] and other measurements to 32 GPa (Ref. 13). However, the experiments of Refs. 13 and 34 were performed without any pressure medium (e.g, nonhydrostatic conditions) and hence are of lower quality. Our results are in reasonable agreement with Ref. 12 especially when one notes that they report anomalous values of the lattice parameters above 30 GPa which require an increase in unit-cell volume for the corundum structure. Above 30 GPa, the a axis is larger than static compression measurements at lower pressure[26] using the trigonal fitting by 0.7–2.7 %. For the monoclinic fitting, the two pseudohexagonal a axes are no longer identical and behave differently: one axis is close to previous studies (0.1–1.6 % larger) but the other axis is 1.0–3.7 % larger. Except for Ref. 34, previously reported c axis shows good agreement below 15 GPa. However, above 20 GPa the difference in the c axis from the extrapolation of lower pressure measurement[26] is generally greater than that in the a axis: 1.4–3.7 % for trigonal fits and 1.8–4.2 % for monoclinic fits. After the phase transition, the Cr_2O_3 structure becomes less compressible along both the c and a axes of pseudohexagonal lattice.

It has been known that the c/a ratio for the corundum-type transition-metal oxides is sensitive to physical property changes.[3,4,35] Below 30 GPa, our c/a ratio in Cr_2O_3 is slightly higher than those of other studies but still in agreement within the experimental scatter (Fig. 7). However, above 30 GPa we observed a 0.4% increase of the c/a ratio for trigonal fits, and 0.5% and 1.5% increase for monoclinic fits. For the monoclinic case, the two c/a ratios diverge with compression.

Since the monoclinic phase and the c/a ratio change were also observed in the pure and Cr-doped V_2O_3 systems and Cr_2O_3 forms a complete solid solution with V_2O_3 (Ref. 36),

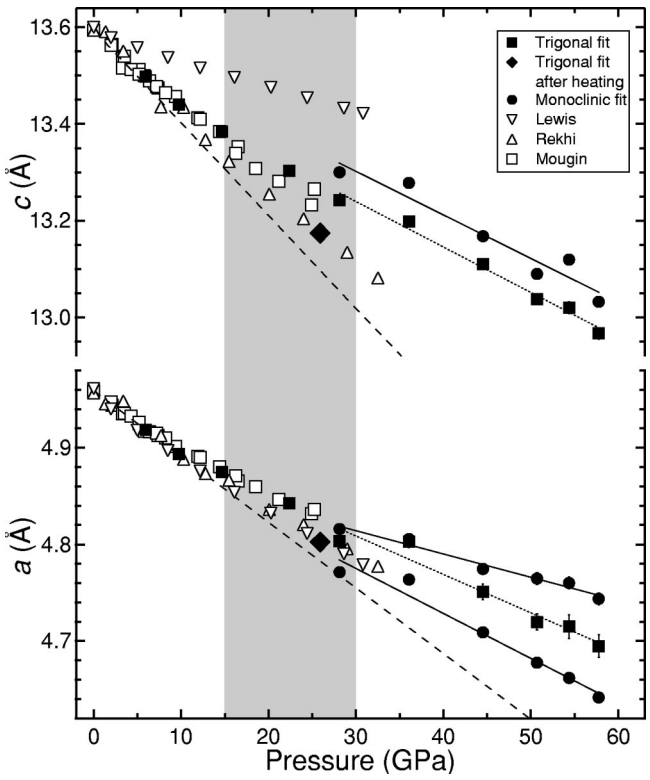

FIG. 6. Pseudohexagonal unit-cell parameters of Cr_2O_3 at high pressure. Trigonal (solid squares) and monoclinic (solid circles) unit-cell parameters were transformed to pseudohexagonal unit-cell parameters to facilitate comparison. Error bars represent 1σ uncertainty. Linear fits for results from monoclinic cell refinements (solid lines) and trigonal cell refinements (dotted lines) are shown. A trigonal fit result for the diffraction pattern measured after laser heating at 25.9 GPa is plotted (solid diamonds). The data points from previous studies (Refs. 12, 13, and 34) are also shown for comparison. Dashed lines are the extrapolation of linear fits for unit-cell parameters measured under hydrostatic stress condition (Ref. 26) below 10 GPa. Due to a severe peak overlap between Cr_2O_3 and argon [$Cr_2O_3(110)_H$ + Ar(111) and $Cr_2O_3(113)_H$ + Ar(200)], only trigonal fit results are shown at 15–27 GPa.

it may be reasonable to compare the current observation with the behavior of the pure and Cr-doped V_2O_3 systems. In pure and Cr-doped V_2O_3, the c/a ratio increase is known to be associated with an insulator-to-metal transition: an antiferromagnetic insulator-to-metal transition at 150 K and ambient pressure in V_2O_3, and a paramagnetic insulator-to-metal transition at 1.1 GPa and 300 K in 4% Cr doped V_2O_3 (Ref. 4). In fact, this systematic trend is also found in Ti_2O_3: a semiconductor-to-metal transition at 390–470 K is accompanied by a 2.1% (from 2.646 to 2.701) c/a ratio increase[3] with temperature. It has been proposed that relative contraction along the pseudohexagonal a axis leads to the formation of bonds between cations in the $(001)_H$ plane of the corundum lattice, resulting in a decrease of resistivity.[2,37] In our study, the c/a ratio increases in Cr_2O_3 at 25–30 GPa (0.4% for the trigonal cell refinement, and 2.0% and 0.5% for the monoclinic refinement).

However, it should be mentioned that the crystal structure

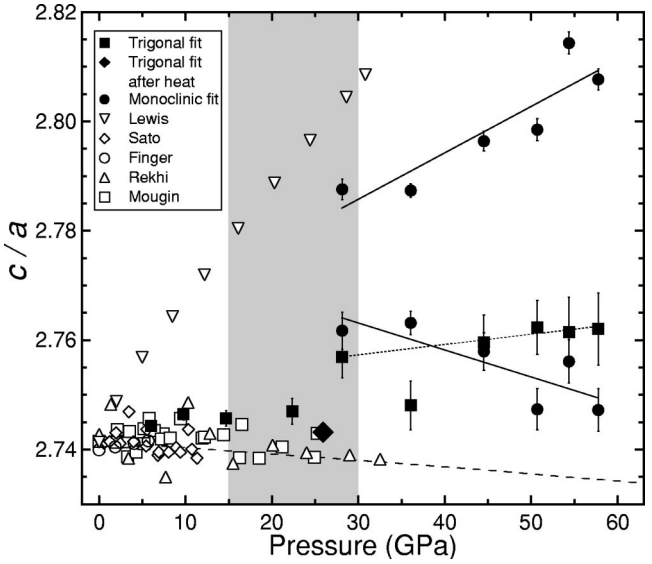

FIG. 7. The c/a ratio of Cr_2O_3 at high pressure. Notations are the same as in Fig. 6. For comparison, we also show the data from lower pressure measurements (Refs. 12, 13, 26, 27, and 34). A data point at 36 GPa from trigonal fit was not included in the linear fit for the c/a vs pressure (dotted line). Due to a severe peak overlap between Cr_2O_3 and argon [$Cr_2O_3(110)_H$ + Ar(111) and $Cr_2O_3(113)_H$ + Ar(200)], only trigonal fits are shown at 15–27 GPa.

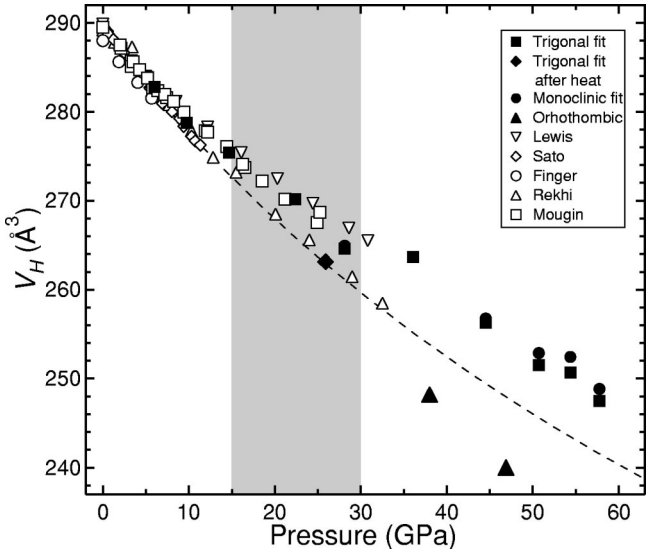

FIG. 8. Volume of Cr_2O_3 transformed to pseudohexagonal unit cell ($Z=6$) at high pressure. Notations are the same as in Fig. 7. The volume of the orthorhombic phase observed after laser heating at 38 and 46.9 GPa is also shown (solid triangles). Dashed curve is the extrapolation of hydrostatic compression (Ref. 26) below 10 GPa at 300 K ($K_{T0}=222$ GPa and $K'_{T0}=4$). Due to a severe peak overlap between Cr_2O_3 and argon [$Cr_2O_3(110)_H$ + Ar(111) and $Cr_2O_3(113)_H$ + Ar(200)], only trigonal fits are shown at 15–27 GPa.

change from the monoclinic to the trigonal in V_2O_3 was observed together with the increase of the c/a ratio, which is the opposite of our observation for Cr_2O_3 at high pressure. The driving force in V_2O_3 is a contraction of structure along the c axis and an elongation along the a axis, while in Cr_2O_3 it occurs in the opposite fashion. Thus, it may not be appropriate to use the increase of the c/a ratio in Cr_2O_3 as a sign of an insulator-metal transition.

The volume change in Cr_2O_3 at high pressure is shown in Fig. 8. Our measurement is consistent with recent x-ray diffraction experiments[12] and slightly higher than the extrapolation of low-pressure hydrostatic measurements.[26] We do not observe a discrete change in volume of any significance, within the observed data scatter, during cold compression for the entire pressure range we studied at 300 K. A recent measurement[12] reported that Cr_2O_3 becomes almost incompressible above 30 GPa. Our data points at 28–36 GPa can be interpreted as being consistent with this observation. However, the change at 28–36 GPa is still within the observed scatter of the data points (Fig. 8). Due to the expected subtle nature of the transition to the monoclinic V_2O_3-type phase and the finite resolution of the high-pressure technique we used, it is difficult to detect the phase transition pressure using the volume data.

B. Phase transition above 30 GPa and high temperature

Drastic changes in Raman spectra were observed after laser heating above 30 GPa (Fig. 9). After heating, wave numbers of Raman modes are different from those observed before heating, and the number of observed modes increases from 9 to 12 (Fig. 10). The latter could mean a structural change to a lower symmetry phase: according to group theory, a total of 24 modes for the perovskite type and 30 modes for the Rh_2O_3-II type are expected to be Raman ac-

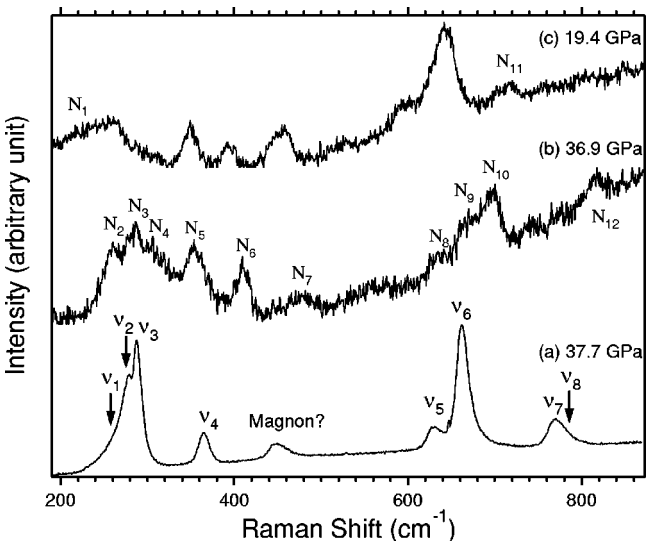

FIG. 9. High-pressure Raman spectra of Cr_2O_3 measured after laser heating (b) and after decompression of the laser-heated sample (c). Raman spectrum without laser heating measured at 37.7 GPa is shown for comparison. New features observed after laser heating at 36.9 GPa are named in sequential order starting from the lowest wave-number peak (N_1–N_{12}). New features observed above 15–30 GPa during cold compression are indicated by arrows (ν_1, ν_2, and ν_8). Pressure is shown above each trace.

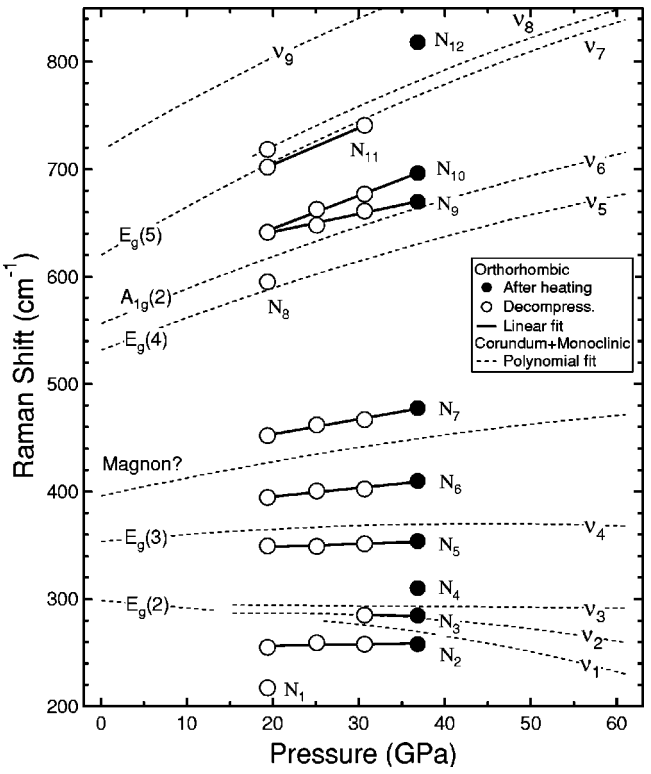

FIG. 10. Pressure shift of Raman modes for the orthorhombic phase of Cr_2O_3. Solid circles are the data points measured after laser heating and open circles are the data points measured during decompression of the laser heated sample. Linear fits for data points are shown as solid lines. For comparison, the positions of Raman modes of the corundum and the monoclinic V_2O_3-type Cr_2O_3 are shown as dotted lines using the polynomial fits presented in Fig. 3. Peak assignments are the same as in Fig. 1.

tive, whereas only 7 for the corundum type and 15 for the monoclinic V_2O_3 type are expected to be Raman active. However, as shown for the orthorhombic phase of Fe_2O_3 above 55 GPa, not all Raman-active modes are observable.[7] In addition, Raman scattering becomes much weaker after heating. It is interesting that decreases in Raman scattering intensities were also observed for the phase transition in Fe_2O_3 at 55 GPa (Ref. 7).

Many of the modes appearing after laser heating (solid circles in Fig. 10) still remain during decompression (open circles in Fig. 10). However, the wave numbers for some modes coincide with those of the modes observed without heating (N_1, N_8, and N_{11} in Fig. 10). Since Raman scattering was much more intense before heating, a small amount of the back-transformed material could show scattering with significant intensities.

Considerable changes were also observed in diffraction patterns after laser heating (Fig. 11): new diffraction lines appear at 3.0, 2.4, and 1.7 Å and intensities of the low *d*-spacing lines change significantly. However, some major diffraction lines of the low-temperature phase (either the corundum or the monoclinic V_2O_3 type) still persist even after laser heating, i.e., diffraction lines at 3.4 and 2.75 Å. This implies that the phase transition to this orthorhombic phase is very sluggish.

The observed diffraction patterns after laser heating can be well explained by an orthorhombic unit cell. We also performed Rietveld analyses for the diffraction patterns of the orthorhombic phase. We used both the Rh_2O_3-II type ($Pbna$, D_{2h}^{14}) and the perovskite-type ($Pbnm$, D_{2h}^{16}) structures as starting models for the analyses. Refinements with both of these models show equally good fit to the peak positions observed after laser heating. However, when we release the constraints for atomic positions in Rietveld analyses, we found very anisotropic Cr-O polyhedra for both the space groups: maximum 42% difference of Cr-O bonds in the octahedra of the Rh_2O_3-II type and maximum 35% difference for Cr-O bonds in the dodecahedra of the perovskite type (we considered nearest eight oxygens, since the perovskite structure with $Pbnm$ space group inherently has distorted dodecahedra such that eight oxygens are closely coordinated around a Cr atom).

These values are rather extreme compared with the reported anisotropy of polyhedra in these structures. For example, for the Rh_2O_3-II-type structures, 5% and 10% anisotropies of octahedra are reported in Rh_2O_3 (Ref. 38) and Fe_2O_3 (Ref. 39) at high pressure, respectively. In the perovskite-type structures, 22% and 21% anisotropies of dodecahedra are reported in $GdFeO_3$ (Ref. 40) and $MgSiO_3$ (Ref. 41) perovskites at ambient pressure, respectively. Thus, the obtained atomic positions for the orthorhombic phase may not be realistic. In fact, for the measurements with laser heating, we used a slot-type aperture of Mao-Bell-type diamond cell. This allows only 8°–10° arc of diffraction rings. Furthermore, recrystallization and preferred orientation induced during laser heating can decrease the accuracy of the measured intensity considerably.[42] These pose severe limits in determination of atomic positions using the measured intensity.

We also performed refinements with quasirigid body constraints for Cr-O polyhedra in the structures: we set limits in the variations of Cr-O bond lengths. For the same allowed variations, the weighted residual factor R_{wp} is slightly better when the perovskite type is used, but the difference is less than 0.2%. For space-group determination, more precise measurements for diffraction intensities are required.

We compare the volume of the orthorhombic phase with those of the corundum and the monoclinic V_2O_3-type phases (Fig. 8). Compared with the compressional curve extrapolated from low-pressure measurements,[26] the orthorhombic structure decreases volume by 2–3 %, whereas the volume decrease is 5–6 %, if compared with that of the monoclinic V_2O_3-type phase. The volume decrease for the corundum-to-Rh_2O_3-II transition is reported to be 3.2% for Rh_2O_3 (Ref. 38) and 10% for Fe_2O_3 (Ref. 39).

IV. DISCUSSION

We observed the sample at each pressure step during Raman and x-ray experiments using an optical microscope. At ambient pressure, Cr_2O_3 has a green color. It becomes darker with compression and turns to dark red near 14 GPa. Above 30 GPa after laser heating, the sample color changed from dark red to dark green. However, below 30 GPa, the sample

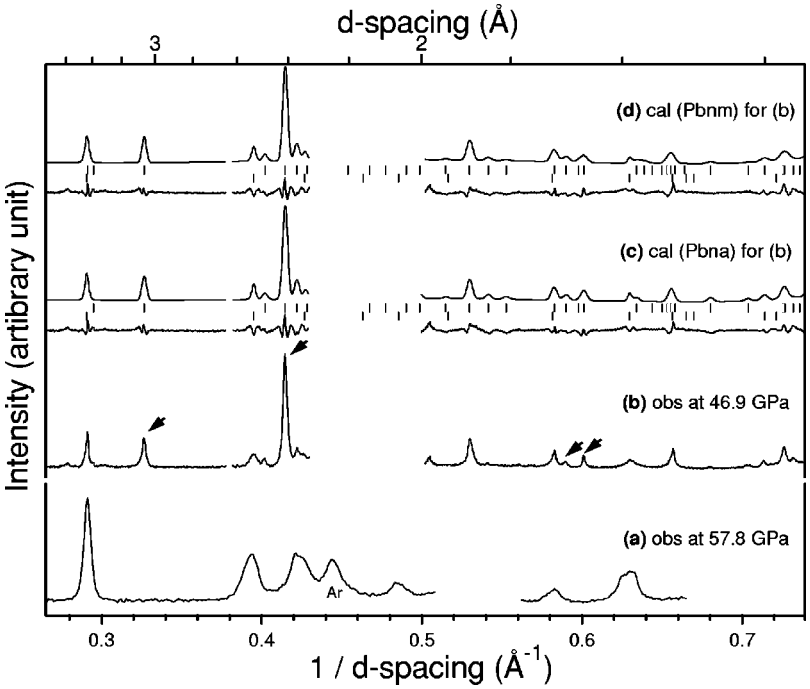

FIG. 11. Observed (a,b) and calculated (c,d) x-ray diffraction patterns at high pressure. The difference between the observed and calculated patterns is also shown for each calculated pattern. Tick marks are the diffraction peak positions for Cr_2O_3 [monoclinic V_2O_3 phase at the bottom of (c) and (d); orthorhombic phase at the top of (c) and (d)]. Backgrounds were subtracted. For comparison, the observed pattern at 57.8 GPa is shown in (a). Two different refinements with the Rh_2O_3-II-type ($Pbna$) (c) and the perovskite-type ($Pbnm$) (d) structures are shown for the pattern measured at 46.9 GPa after laser heating (b). The data points at 0.378–0.382 Å^{-1} and 0.430–0.502 Å^{-1} were not used in the refinements due to the overlaps with gasket peaks. The arrows indicate distinct major diffraction features of the orthorhombic phase.

still shows a dark red color even after laser heating. These visual observations, together with Raman scattering and x-ray diffraction, show that there exist changes in the compressional behavior of Cr_2O_3 at high pressure.

Colors in $3d$-transition metal sesquioxides are related to the crystal-field splitting of their $3d$ orbitals.[43] This splitting depends on cation-anion bond lengths and symmetry of the cation site. In an ideal octahedron, degenerated d-orbitals split into t_{2g} and e_g orbital groups energetically. The energy separation of these, Δ, can be expressed as a function of average cation-anion separation R,

$$\frac{\Delta}{\Delta_0} = \left(\frac{R_0}{R}\right)^5, \tag{2}$$

assuming that there is no change in the symmetry of the octahedron. Using this relation, we calculated an average cation-anion separation needed for Cr_2O_3 to show same Δ as ruby ($\Delta = 18\,150$ cm^{-1}, Ref. 44). For $\Delta_0 = 16\,670$ cm^{-1} (Ref. 45) and $R_0 = 1.986$ Å, we obtained $R = 1.952$ Å. This corresponds to the Cr-O length at 14 GPa where the color change from green to red is observed [Fig. 12(a)], implying that the color change is induced by the compression of CrO_6 octahedra.

However, the color of Cr_2O_3 changes back to green after laser heating above 30 GPa. We found that average Cr-O distance increases when Cr_2O_3 transforms to the orthorhombic phase. If ruby transforms from the corundum structure to the orthorhombic structure above 100 GPa as predicted[8,9] and the phase transition is similar to that in Cr_2O_3 as proposed by the first-principles study,[10] this discrete change in crystal-field energy during the phase transition to the orthorhombic phase could result in a significant change in the ruby scale.

In order to further investigate the source of the crystal structure change, we plot measured Cr-O and O-O bond lengths as a function of pressure (Fig. 12). These values are obtained from Rietveld analyses of the diffraction patterns measured at high pressure and 300 K, with and without laser annealing, using the corundum structure. The monoclinic V_2O_3 structure can be thought as a distorted corundum structure with small differences including the absence of threefold axes along the c axis of the trigonal unit cell in the monoclinic structure. Unfortunately, our diffraction experiments do not cover sufficient reciprocal space to refine the individual oxygen positions in the monoclinic structure. Thus, we use the results from the refinements with the corundum structure, which has only one atomic position parameter to be refined for oxygen, instead in the monoclinic V_2O_3 structure four oxygen position parameters should be refined. Use of these results may lead to systematic errors in the measured bond lengths above 30 GPa where significant misfits of the observed diffraction patterns with the corundum structure are observed (Fig. 5). However, the misfits are not significant below 30 GPa. Also the observed trend is still preserved even after laser heating near 30 GPa [diamond symbols in Figs. 12(a) and 12(c)] where differential stress should be much smaller. In addition, the trends observed in our data are very consistent with that observed in single-crystal diffraction experiments[27] below 6 GPa [Fig. 12(a)].

Oxygens in the corundum structure are hexagonally close packed. Two-thirds of the octahedral interstitial sites are filled with cations and one-third of the sites remain empty. Along the c axis, two cation-filled octahedra share one oxygen plane (''shared'' by two cations above and below; represented by subscript ''s'') and one empty octahedron shares an oxygen plane with one filled octahedron (''unshared''; represented by subscript ''u''). At ambient pressure, M-O_s (M: cation, M = Al, V, Cr, Fe) is longer than M-O_u. However, in both single-crystal and our powder-diffraction measurements, the Cr-O_s bond length decreases rapidly with

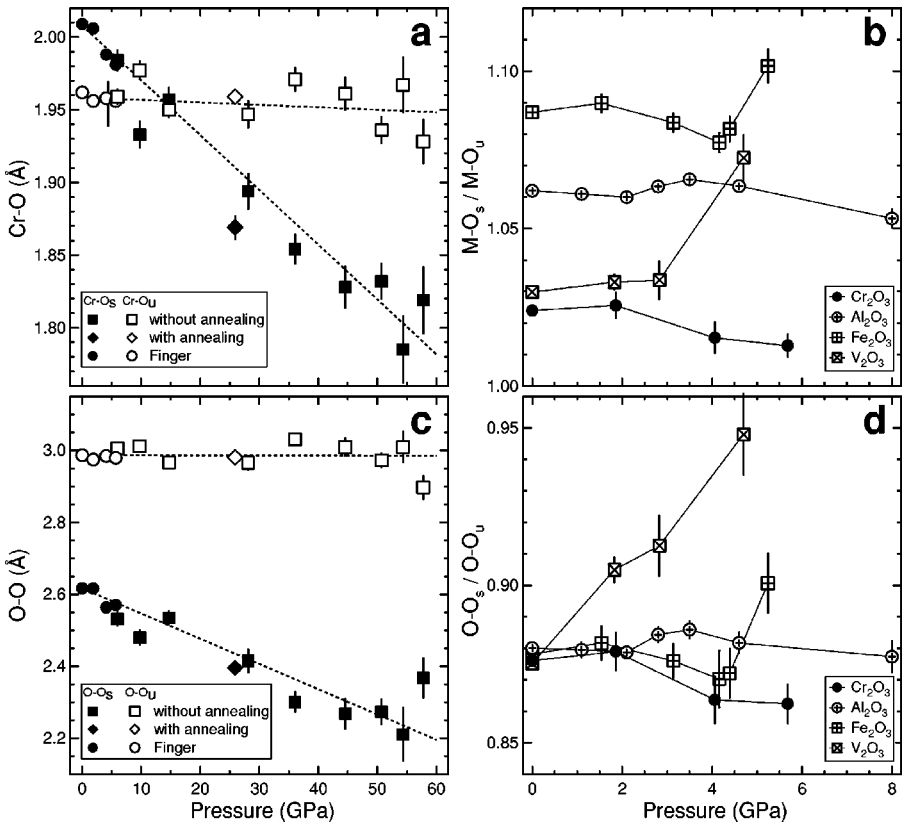

FIG. 12. (a) Cr-O and (c) O-O bond lengths in the corundum-type Cr_2O_3 measured at high pressure and 300 K. Bond lengths between Cr and O in both shared (subscript "*s*," solid symbols) and unshared (subscript "*u*," open symbols) oxygen layers are shown for measurements both with (diamonds) and without (squares) laser annealing. The measured values by a single-crystal x-ray diffraction (Ref. 27) are also plotted for comparison (circles). The dotted lines are for guides for the eye. We compared (b) cation-oxygen (M–O) and (d) oxygen-oxygen (O–O) bond length ratios between oxygens in shared and unshared oxygen planes in different corundum-type sesquioxides at high pressure and 300 K. The values are obtained from single-crystal x-ray-diffraction measurements (Refs. 46 and 27).

compression, whereas Cr-O_u is very insensitive to compression. In fact, these two Cr-O bond lengths are almost identical near 15 GPa and the Cr-O_s bond length becomes smaller than the Cr-O_u bond length above 20 GPa. Although it is difficult to see the trend in single-crystal diffraction measurements due to their limited pressure range, the decrease of the M-O_s bond length relative to the M-O_u bond length can be found in the data for Cr_2O_3 [Fig. 12(b)].

In the corundum structure, cations are not at the center of octahedra, instead they are offset from the center along the *c* axis. Thus, the shift of Cr with compression toward the shared oxygen plane could result in the observed decrease in Cr-O_s. However, as shown in Fig. 12(c), it is the decrease of the O-O bond length in the shared oxygen plane, i.e., decrease in the size of the plane, that gives rise to the decrease in Cr-O_s bond length. In other words, the shift of oxygens in the shared plane towards the center of the triangle results in the decrease in Cr-O_s bond length. Interestingly, the size of the unshared oxygen plane is very insensitive to pressure. Also this relative decrease in O-O_s bond length can be seen in single-crystal diffraction measurements [Fig. 12(d)].

Recent first-principles calculations[10,11] have proposed that Cr_2O_3 will show a similar phase transition to that in Al_2O_3 at much lower pressure. It is difficult to compare the pressure behavior of bond lengths in Al_2O_3 with those in Cr_2O_3, since only a single-crystal x-ray diffraction measurement with a limited pressure range is available. However, Fig. 12(b) and 12(c) show that the bond lengths in Al_2O_3 follow a more or less similar trend to those in Cr_2O_3. In contrast, Fe_2O_3 and V_2O_3 show opposite pressure behaviors in bond lengths.

It is interesting that there is difference in transition pressures detected by Raman scattering and x-ray diffraction for the corundum-to-monoclinic V_2O_3 phase transition: whereas two new Raman modes are observed from 15 GPa (Fig. 3), the c/a ratio measured by x-ray diffraction shows a discrete increase at 25–28 GPa (Fig. 7). It should be noted that the expected changes in the phase transition are subtle. Furthermore, we have a finite resolution in both Raman and x-ray-diffraction measurements, due to stress inhomogeneity, nonhydrostatic stresses, and so on. In fact, the two new modes (ν_2 and ν_8 in Fig. 3) are not fully resolved to 30 GPa and these appear only as asymmetricity of modes ν_3 and ν_7. Furthermore, ν_1 is resolved above 30 GPa which is rather close to where the c/a ratio change is found in diffraction experiments.

We also investigated whether the monoclinic V_2O_3 phase is induced by nonhydrostatic stresses in the sample. In fact, there is some evidence for the existence of differential stresses in our experiments: the volume measured without laser annealing above 15 GPa is 1% higher than that extrapolated from low-pressure hydrostatic experiments[26] and that measured after annealing at 26 GPa (Fig. 8). Also, the FWHM of diffraction peaks measured during cold compression is significantly larger than that measured after laser annealing (Fig. 11). In contrast, the bond distance change (Fig. 12) in an annealed sample at 26 GPa is in good agreement with those in cold compressed samples, and the Raman features observed before annealing are still preserved after annealing at 26 GPa. A measurement with quasihydrostatic medium, e.g., helium, is warranted to resolve this issue. The

monoclinic V_2O_3-type phase is metastable above 30 GPa where a 5–6 % more dense phase, the orthorhombic phase, exists (Fig. 8).

V. CONCLUSION

We have observed a color change, splittings of Raman modes, relative increases of some Raman mode intensities, selective broadening of some diffraction lines, and systematic shifts of some diffraction positions in Cr_2O_3 at 15–30 GPa. The Raman spectrum and diffraction changes are consistent with a phase transition to the monoclinic V_2O_3 structure ($I2/a$), which has also been observed in pure and Cr-doped V_2O_3 systems, but the observed changes are not consistent with a phase transition to the orthorhombic structure (Rh_2O_3-II or perovskite type). The phase transition may be induced by the different compressibility of cation-filled and empty octahedra in Cr_2O_3.

We also find another phase transition above 30 GPa and after laser heating. The high-temperature phase has an orthorhombic unit cell as predicted by first-principles calculations[10] and Rietveld refinement shows that this could be either the Rh_2O_3-II or the perovskite-type structure. The color change during this phase transition, from dark red to green, is consistent with the fact that average Cr-O bond length increases after the phase transition. Since the orthorhombic phase has much smaller volume than the monoclinic V_2O_3-type phase, the orthorhombic phase is more stable than the monoclinic phase above 30 GPa. It is interesting that the monoclinic V_2O_3-type phase survives metastably over a wide pressure range (30–60 GPa).

Since it has been proposed that the phase transition in Cr_2O_3 is similar to that expected in ruby,[10,11] the phase transitions found in this study may have important implications for the ruby scale. This study shows that the phase transitions in Cr_2O_3 are accompanied with changes in both cation-anion bond length and cation site symmetry, which are important factors to influence the crystal-field splitting energy whose pressure variation is used in the ruby scale.

ACKNOWLEDGMENTS

S. Speziale, C. Zha, K. Lee, and G. Shen assist x-ray measurements. This work was supported by NSF. S.S. and R.J. thank the Miller institute for support.

*Electronic address: sangshim@mit.edu

[1] P. A. Cox, *Transition Metal Oxides—an Introduction to their Electronic Structure and Properties*, International Series of Monographs on Chemistry Vol. 27 (Oxford Science Publications, Oxford, 1992).
[2] A. Mooradian and P.M. Raccah, Phys. Rev. B **3**, 4253 (1971).
[3] C.N.R. Rao, R.E. Loehman, and J.M. Honig, Phys. Lett. **27A**, 271 (1968).
[4] D.B. McWhan and J.P. Remeika, Phys. Rev. B **2**, 3734 (1970).
[5] P.D. Dernier and M. Marezio, Phys. Rev. B **2**, 3771 (1970).
[6] M.P. Pasternak, G.K. Rozenberg, G.Y. Machavariani, O. Naaman, R.D. Taylor, and R. Jeanloz, Phys. Rev. Lett. **82**, 4663 (1999).
[7] S.-H. Shim and T.S. Duffy, Am. Mineral. **87**, 318 (2002).
[8] K.T. Thomson, R.M. Wentzcovitch, and M.S.T. Bukowinski, Science **274**, 1880 (1996).
[9] N. Funamori and R. Jeanloz, Science **278**, 1109 (1997).
[10] W. Duan, G. Paiva, R.M. Wentzcovitch, and A. Fazzio, Phys. Rev. Lett. **81**, 3267 (1998).
[11] A.Y. Dobin, W. Duan, and R.M. Wentzcovitch, Phys. Rev. B **62**, 11 997 (2000).
[12] J. Mougin, T.L. Bihan, and G. Lucazeau, J. Phys. Chem. Solids **62**, 553 (2001).
[13] S. Rekhi, L.S. Dubrovinsky, R. Ahuja, S.K. Saxena, and B. Johansson, J. Alloys Compd. **302**, 16 (2000).
[14] H.-K. Mao, J. Xu, and P.M. Bell, J. Geophys. Res. **91**, 4673 (1986).
[15] L.W. Finger, R.M. Hazen, G. Zou, H.-K. Mao, and P.M. Bell, Appl. Phys. Lett. **39**, 892 (1981).
[16] S. Desgreniers, University of Ottawa, Technical Report, 1998 (unpublished).
[17] T.J.B. Holland and S.A.T. Redfern, Miner. Mag. **61**, 65 (1997).
[18] A. C. Larson and R. B. V. Dreele, Los Alamos National Laboratory, Technical Report No. LAUR 86-748, 1988 (unpublished).
[19] G. Shen, M.L. Rivers, Y. Wang, and S.R. Sutton, Rev. Sci. Instrum. **72**, 1273 (2001).
[20] I.R. Beattie and T.R. Gilson, J. Chem. Soc. A **5**, 980 (1970).
[21] T. R. Hart, R. L. Aggarwal, and B. Lax, in *Proceedings of the Second International Conference on Light Scattering in Solids*, edited by M. Balkanski (Flammarion Sciences, Paris, 1971), pp. 174–179.
[22] C. Tatsuyama and H.Y. Fan, Phys. Rev. B **21**, 2977 (1980).
[23] K.F. McCarty and D.R. Boehme, J. Solid State Chem. **79**, 19 (1989).
[24] N. Kuroda and H.Y. Fan, Phys. Rev. B **16**, 5003 (1977).
[25] D. Bloch, J. Phys. Chem. Solids **27**, 881 (1966).
[26] Y. Sato and S. Akimoto, J. Appl. Phys. **50**, 5285 (1979).
[27] L.W. Finger and R.M. Hazen, J. Appl. Phys. **51**, 5362 (1980).
[28] M.C. Aronson, S.B. Dierker, B.S. Dennis, S.-W. Cheong, and Z. Fisk, Phys. Rev. B **44**, 4657 (1991).
[29] V.V. Struzhkin, A.F. Goncharov, and K. Syassen, Mater. Sci. Eng., A **168**, 107 (1993).
[30] V.V. Struzhkin, U. Schwarz, H. Wilhelm, and K. Syassen, Mater. Sci. Eng., A **168**, 103 (1993).
[31] E.J. Samuelsen, Physica (Amsterdam) **43**, 353 (1969).
[32] G. Lucovsky, R.J. Sladek, and J.W. Allen, Phys. Rev. B **16**, 4716 (1977).
[33] A.F. Reid and A.E. Ringwood, J. Geophys. Res. **74**, 3238 (1969).
[34] H.J. Lewis, Jr. and H.G. Drickamer, J. Chem. Phys. **45**, 224 (1966).
[35] C.T. Prewitt, R.D. Shannon, D.B. Rogers, and A.W. Sleight, Inorg. Chem. **8**, 1985 (1969).
[36] R. S. Roth, *Phase Equlibria Diagrams-Phase Diagrams for Ceramists* (The American Ceramic Society, 1995).
[37] J. B. Goodenough, *Magnetism and the Chemical Bond* (Robert E. Krieger, New York, 1976).
[38] R.D. Shannon and C.T. Prewitt, J. Solid State Chem. **2**, 134 (1970).

[39] G.K. Rozenberg, L.S. Dubrovinsky, M.P. Pasternak, O. Naaman, T.L. Bihan, and R. Ahuja, Phys. Rev. B **65**, 064112 (2002).
[40] S. Geller, J. Chem. Phys. **24**, 1236 (1956).
[41] H. Horiuchi, E. Ito, and D.J. Weidner, Am. Mineral. **72**, 357 (1987).
[42] S.-H. Shim, R. Jeanloz, and T.S. Duffy, Geophys. Res. Lett. **29**, 2166 (2002).
[43] R. G. Burns, *Mineralogical Applications of Crystal Field Theory* (Cambridge University Press, New York, USA, 1993).
[44] R.M. Macfarlane, J. Chem. Phys. **39**, 3118 (1963).
[45] D.S. McClure, J. Chem. Phys. **38**, 2289 (1963).
[46] L.W. Finger and R.M. Hazen, J. Appl. Phys. **49**, 5823 (1978).